Liu et al. Nanoscale Research Letters (2016) 11:159
DOI 10.1186/s11671-016-1372-2

Nanoscale Research Letters

NANO EXPRESS Open Access

Porous TiO_2 Assembled from Monodispersed Nanoparticles

Xu Liu, Weijie Duan, Yan Chen, Shihui Jiao, Yue Zhao, Yutang Kang, Lu Li, Zhenxing Fang, Wei Xu and Guangsheng Pang*

Abstract

Porous TiO_2 were assembled by evaporating or refluxing TiO_2 colloid, which was obtained by dispersing the TiO_2 nanoparticles with a crystallite size (d_{XRD}) of 3.2 nm into water or ethanol without any additives. Porous transparent bulk TiO_2 was obtained by evaporating the TiO_2-C_2H_5OH colloid at room temperature for 2 weeks, while porous TiO_2 nanospheres were assembled by refluxing the TiO_2-H_2O colloid at 80 °C for 36 h. Both of the porous TiO_2 architectures were pore-size-adjustable depending on the further treating temperature. Porous TiO_2 nanospheres exhibited enhanced photocatalysis activity compared to the nanoparticles.

Keywords: TiO_2 nanoparticles, Porous TiO_2, Assemblies, Photodegradation

Background

Size plays an outstanding role in determining the properties of materials. After several decades of intense research on size effects of single nanoparticle or small nanoparticle clusters, the trend goes in the direction of meso- and macroscale structures consisting of nanoscale building blocks [1]. Nanoparticles, which possess the characters of small size and large surface area, have received widely attention due to their unique properties of optics, magnetics, electrics and catalysis [2–5]. To expand the research on nanoparticles, there has been growing interest in constructing hierarchical structures consisting of aggregated nanoparticles [6–8]. The combination of size effects and collective properties gives rise to fascinating opportunities for the creation of unprecedented materials. It is important to control the organization and dispersion states to assemble nanomaterials [9–11]. For example, the homogeneous and disordered assembly of densely packed nanoparticles can result in bulk transparent film-like objects through gradually evaporating the high-quality homogeneous nanoparticle colloid [12, 13]. The high transmittance benefits from the homogeneous particles, which are quite small and do not scatter visible light. The homogeneous assembly of densely packed nanoparticles results in a narrow range of pore sizes that are highly dependent on the size and uniformity of the nanoparticles [14, 15].

As a most promising photocatalyst, anatase TiO_2 has been widely investigated to improve its photocatalytic performance. Porous TiO_2 has performed much higher photocatalytic activity than solids due to their stronger adsorption to substrates and/or higher light-harvesting ability [16–19]. The void space can modulate the refractive index, lower the density, increase the active area for catalysis and improve the catalysts' ability to withstand cyclic changes in volume. Furthermore, void space in hollow structures can be used to encapsulate and control release of sensitive materials such as drugs and cosmetics. TiO_2 nanomaterials with different morphologies have been reported, and it is still a challenge to assemble TiO_2 nanoparticles (TiO_2-NPs) to form a porous structure [20–22].

In our study, monodispersed anatase TiO_2-NPs were prepared by the hydrolysis of tetrabutyltitanate (TBT) in a cyclohexane/ethanol medium. The assembly of TiO_2-NPs was investigated under different conditions and resulted in transparent bulk TiO_2 and porous TiO_2 nanospheres (TiO_2-NSs).

* Correspondence: panggs@jlu.edu.cn
State Key Laboratory of Inorganic Synthesis and Preparative Chemistry, College of Chemistry, Jilin University, Changchun, Jilin 130012, People's Republic of China

Methods

Preparation of TiO_2-NPs

All of the chemicals were of analytic grade and used without further purification. We prepared TiO_2 nanoparticles by the hydrolysis of tetrabutyltitanate (TBT) in a cyclohexane (C_6H_{12})/ethanol (C_2H_5OH) medium under refluxing conditions as reported [23]. Briefly, 36 mL of TBT was dissolved in the mixed solvents (90 mL of ethanol and 90 mL of cyclohexane), and 9 mL of HCl (TBT/HCl (v/v) = 1:0.25) was added to it. The final homogeneous solution was refluxed at 67 °C for 10 h and then cooled to room temperature. To precipitate the TiO_2-NPs, 600 mL of ethanol was added dropwise to the solution under stirring. After standing overnight, a white precipitate was harvested by centrifugation. The powder was obtained by washing with ethanol three times and dried in air at room temperature. (Additional file 1 shows the X-ray diffraction (XRD) pattern, transmission electron microscopy (TEM) image and the size distribution histogram of TiO_2-NPs).

Preparation of the Porous Transparent Bulk TiO_2

Ten milligrams of freshly prepared TiO_2-NPs was added to 10 mL of ethanol in a 1000-mL beaker covered with plastic wrap. After standing for 2 days, the turbid suspension gradually changed to a transparent TiO_2-C_2H_5OH colloid. Porous transparent bulk TiO_2 was obtained by evaporating the TiO_2-C_2H_5OH colloid at room temperature for 2 weeks. To investigate the thermal stability, porous transparent bulk TiO_2 was heated at different temperatures for 2 h with a heating rate of 5 °C/min in air.

Preparation of TiO_2-NSs

The freshly prepared TiO_2-NPs were dispersed into deionized water to form a TiO_2-H_2O colloid. Typically, 100 mL of a 10-g/L TiO_2-H_2O colloid was heated at 80 °C for 36 h. Then, the precipitate was collected by centrifugation, washed with deionized water several times, and dried in air at room temperature. The thermal stability of the TiO_2-NSs was studied by heating at different temperatures for 2 h with a rate of 5 °C/min in air.

Characterization

Powder XRD patterns were recorded on a PANalytical B.V. Empyrean X-ray diffractometer with graphite-filtered Cu $K\alpha$ radiation at 40 kV and 40 mA. A SU8020 electron microscope was applied to get scanning electron microscopy (SEM) images. High-resolution transmission electron microscopy (HRTEM) was performed on a Tecnai G2 S-TWIN F20 at an accelerating voltage of 200 kV. Before being studied by HRTEM, porous transparent bulk TiO_2 specimens were fabricated on an FEI Helios NanoLab 600i FIB/SEM dual-beam system. Infrared (IR) spectra of the samples were recorded on a Bruker IFS-66V/S FT-IR spectrometer with a resolution of 2 cm^{-1}. Thermogravimetric analysis (TG) was carried out on a NETZSCH STA 449 F3 with a heating rate of 20 K/min from room temperature to 800 °C. Brunauer-Emmett-Teller (BET) measurements were performed via the nitrogen adsorption method on a Micromeritics ASAP 2420, and UV-Vis absorption was measured on a UV-2450 spectrophotometer.

Photodegradation

The photocatalytic activity of TiO_2-NPs and TiO_2-NSs was tested by measuring the degradation rate of methylene blue (MB) under UV light irradiation. Typically, 50 mg of the as-prepared TiO_2 catalyst was added to 50 mL of an aqueous solution containing 10 mg/L MB. The mixture was magnetically stirred in the dark at ambient temperature for 1 h to achieve adsorption-desorption equilibrium of TiO_2 with MB followed by exposure to UV light from a 125-W high-pressure mercury vapour lamp. Five milliliters of the suspension was extracted every 10 min, and the suspended solid was immediately separated by centrifugation. UV-Vis absorption spectra were measured to monitor the concentration of MB remaining in the aqueous system. For comparison, Degussa P25 was adopted to investigate the photocatalytic activity under the same condition.

Results and Discussion

The Assembly of Porous Transparent Bulk TiO_2

When freshly prepared TiO_2-NPs with a crystallite size (d_{XRD}) of 3.2 nm (see Additional file 1) were dispersed in ethanol, the turbid suspension gradually became a transparent TiO_2-C_2H_5OH colloid after standing for 2 days. The digital photographic image is shown in Fig. 1a. After evaporating at room temperature, the colloid slowly condensed and formed porous transparent objects with size of 1–3 cm as shown in Fig. 1b. The IR spectrum and TG analysis of the porous transparent bulk TiO_2 are present in Additional file 1: Figure S4 and Figure S5. IR spectrum (Additional file 1: Figure S4) shows the absorption peaks corresponding to the surface

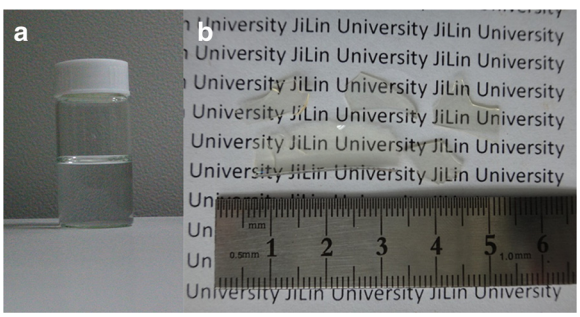

Fig. 1 Digital photographic images of (**a**) TiO_2-C_2H_5OH colloid; (**b**) porous transparent bulk TiO_2

hydroxy group (Ti-O-H) and/or water molecules (O-H stretching mode at ~3200 cm^{-1} and O-H bending mode at ~1620 cm^{-1}). TG analysis (Additional file 1: Figure S5) shows the weight losses from room temperature to 200 °C or higher, which indicates the loss of physically adsorbed water and the surface hydroxy groups. The hydrated layer formed around the nanoparticles and their hydrophilic nature leads to the formation of homogeneous and closely packed nanocrystals [12]. The nanoparticles dispersed in ethanol were homogeneously assembled into bulk materials after the evaporation of ethanol without the formation of inhomogeneous aggregates. During evaporation, TiO_2-NPs in the colloid were drawn to the meniscus by convective transport; capillary forces pushed the organization of close-packed structures [24]. Figure 2a shows the SEM image of the smooth surface; no grain boundaries or cracks were observed on micrometre scale of the bulk objects. The micropores in porous transparent bulk TiO_2 are confirmed by TEM (Fig. 2d) and N_2 physisorption measurements and are formed in the interspaces of the densely packed TiO_2-NPs.

Figure 3b shows the N_2 adsorption-desorption isotherms and the corresponding pore size distribution curves of porous transparent bulk TiO_2. The curve indicates a sharp uptake at low relative pressures and gradually increasing uptake at higher relative pressures. The adsorption isotherm is of type I according to the IUPAC classification, which indicates the presence of micropores [25]. The specific surface area of porous transparent bulk TiO_2 was 197 m^2/g, and the main pore size was located around 1.3 nm. This result agrees well with the homogenous and disordered assembly of nanoparticles in the porous transparent bulk TiO_2.

The as-prepared porous transparent bulk TiO_2 was thermally stable up to 500 °C. No grain boundaries or cracks on micrometre scale were observed (Fig. 2b). After heating at 800 °C for 2 h, boundaries were observed on the surface of the objects using SEM, as shown in Fig. 2c, and the phase was transformed from anatase to rutile during the thermal treatment (Fig. 3a). The BET specific surface decreased, and the pore size gradually increased with heating temperature. The shape of the isotherm of the sample heated above 400 °C turns to type IV with type H2 hysteresis as shown in Fig. 3e, f. This result is consistent with the transformation of pore size from microporosity to mesoporosity as given in Table 1. After heating at 500 °C, the BET specific surface area decreased to 39 m^2/g, and the pore size was 6.9 nm, which indicates that the pore size of porous

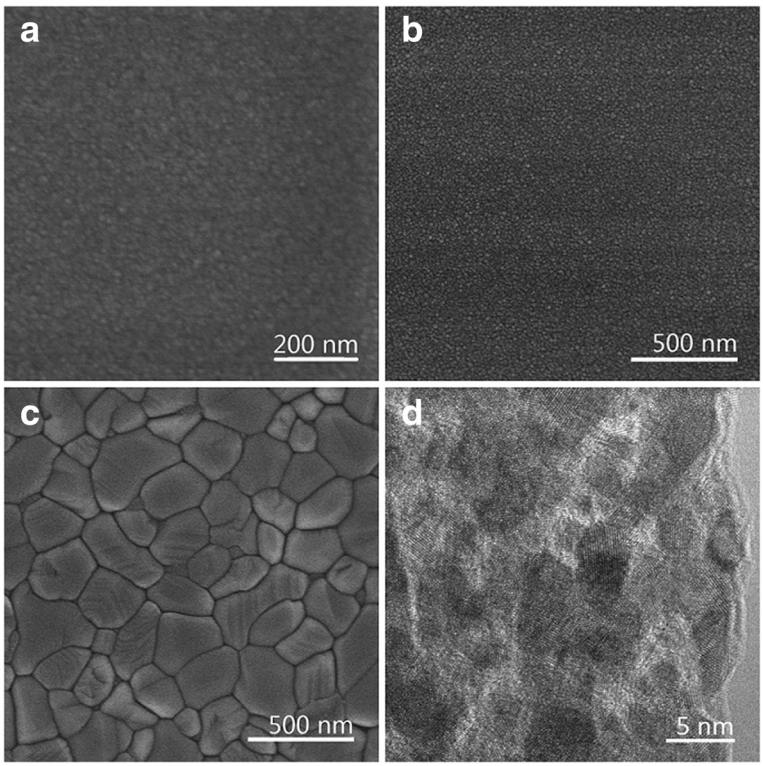

Fig. 2 SEM and TEM images of porous transparent bulk TiO_2. **a** SEM image of the untreated porous transparent bulk TiO_2. **b** SEM image of porous transparent bulk TiO_2 heating at 500 °C. **c** SEM image of porous transparent bulk TiO_2 heating at 800 °C. **d** TEM image of porous transparent bulk TiO_2

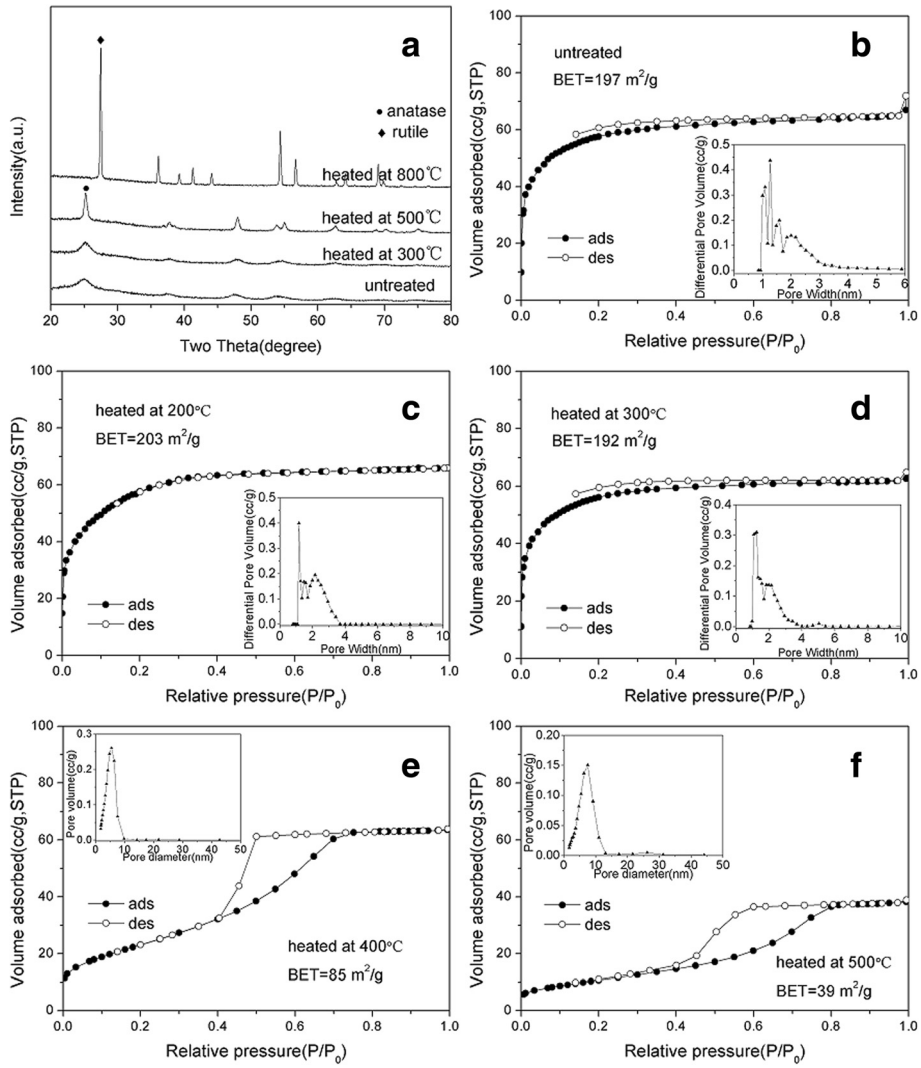

Fig. 3 **a** XRD patterns of porous transparent bulk TiO_2. **b**–**f** N_2 adsorption-desorption isotherms and pore size distribution curves of porous transparent bulk TiO_2 heated at various temperatures

transparent bulk TiO_2 was adjustable from microporous to mesoporous via thermal treatment.

The Assembly of TiO_2-NSs

Freshly prepared TiO_2-NPs can be dispersed into deionized water to form a colloid without any additives [23], and porous TiO_2-NSs can be prepared by heating 10 g/L TiO_2-H_2O colloid at 80 °C for 36 h. The SEM image of the TiO_2-NSs is shown in Fig. 4a, and the results indicate that the nanoparticles assembled into spheres due to the heat treatment. The assembled spheres had a spherical diameter of 100–270 nm. Detailed information of a single TiO_2-NS was provided by TEM (Fig. 4b). The nanospheres had a rough surface and were assembled by nanoparticles (Fig. 4c). In addition, the porous interior is shown in Fig. 4b, c. As revealed in the TEM images, the spheres were composed of TiO_2-NPs.

Table 1 Specific surface area and pore size of porous transparent bulk TiO_2 heated at various temperatures

Sample	Specific surface area (m^2/g)	Average pore size (nm)
Untreated	197	1.3
Heated at 200 °C	203	1.6
Heated at 300 °C	192	1.8
Heated at 400 °C	85	5.4
Heated at 500 °C	39	6.9

The HRTEM micrograph shown in Fig. 4d indicates that each nanoparticle was fully crystallized with a grain size (d_{TEM}) of *ca.* 5 nm. The result is consistent with the analysis of XRD data of untreated TiO_2-NSs shown in Fig. 5a, which is assigned to anatase TiO_2 (JCPDS card no. 21-1276) with crystallite size (d_{XRD}) of 4.6 nm. Heating treatment in the water encouraged the grain growth

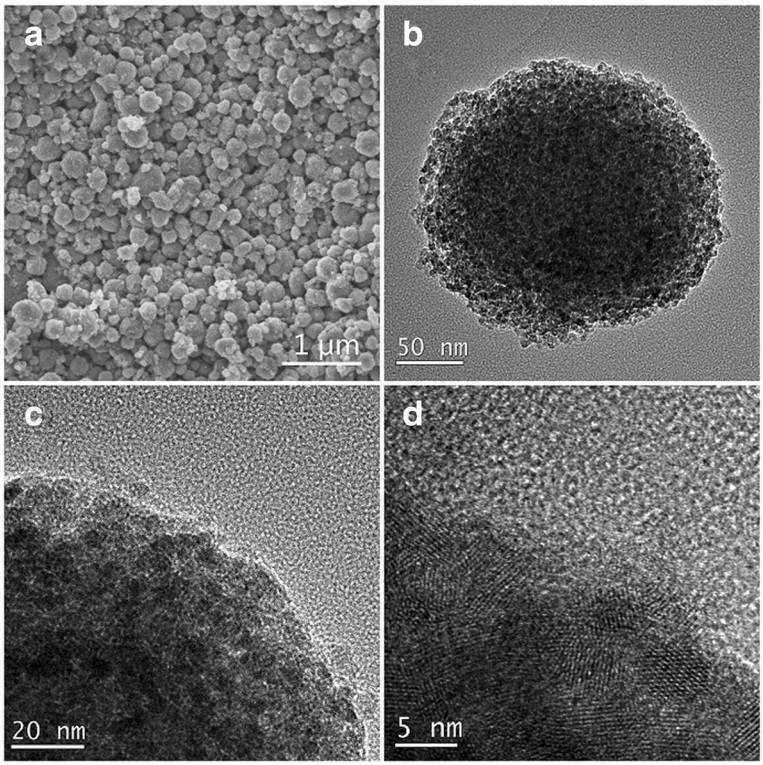

Fig. 4 **a** SEM image. **b**, **c** TEM images. **d** HRTEM image of assembled TiO_2-NSs

due to the Ostwald ripening mechanism and resulted in a larger crystallite size of 4.6 nm compared to the original size of 3.2 nm.

The pore size of the TiO_2-NSs was confirmed by N_2 physisorption measurements. Figure 5b–f shows the N_2 adsorption-desorption isotherms (type IV) [25] and the corresponding pore size distribution curves of the samples heated under different temperatures. The BET specific surface area of the untreated sample was 169 m^2/g, and the average pore size was 1.9 nm (Fig. 5b), which was larger than the transparent bulk TiO_2 due to the bigger crystallite size of the units. After heating at different temperatures, the BET specific surface area and pore size of the assembled nanospheres changed gradually, which can also be ascribed to the increase of the crystallite size, as shown in Table 2. The TiO_2-NSs heated at 600 °C exhibited the largest pore size (6.4 nm), and the untreated TiO_2-NSs exhibited the largest BET specific surface area (169 m^2/g).

Photocatalytic Activities of TiO_2-NPs and TiO_2-NSs

The photocatalytic activities of TiO_2-NPs and TiO_2-NSs were evaluated by the degradation of MB under UV light irradiation. As shown in Fig. 6, the photocatalytic result indicates that the photocatalytic performance was substantially improved after the assembly of TiO_2-NPs into TiO_2-NSs. MB was almost completely removed in 40 min by the TiO_2-NSs heated at 400 °C, which exhibit superior performance among the photocatalysts we studied, including P25.

The number of effective active sites on the surface is an important character of the activity of a photocatalyst, which would be affected by many factors. Photocatalysts with smaller particle size usually exhibit higher activity. The reason may be that when the particle size is smaller, the specific surface area is larger, and more photocatalysis active sites are available. Whereas, when the particle size is too small, most of the electrons and holes are generated close to the surface and surface recombination is faster than interfacial charge carrier transfer processes. It is reported that when the particle size of TiO_2 is smaller than 10 nm, the photocatalytic activity will decrease [26, 27]. But the crystallite size (d_{XRD}) of as-prepared TiO_2-NSs in this work was 4.6 nm which is far less than 10 nm. In addition, the spheres were assembled from nanoparticles by the heat treatment. Surface states play an important role in the recombination process of electron and hole [28]. We believe that the effective contact among nanoparticles affected the surface states which could reduce the recombination chance of electron and hole. Therefore, the photocatalytic activity of TiO_2-NSs improved compared to TiO_2-NPs.

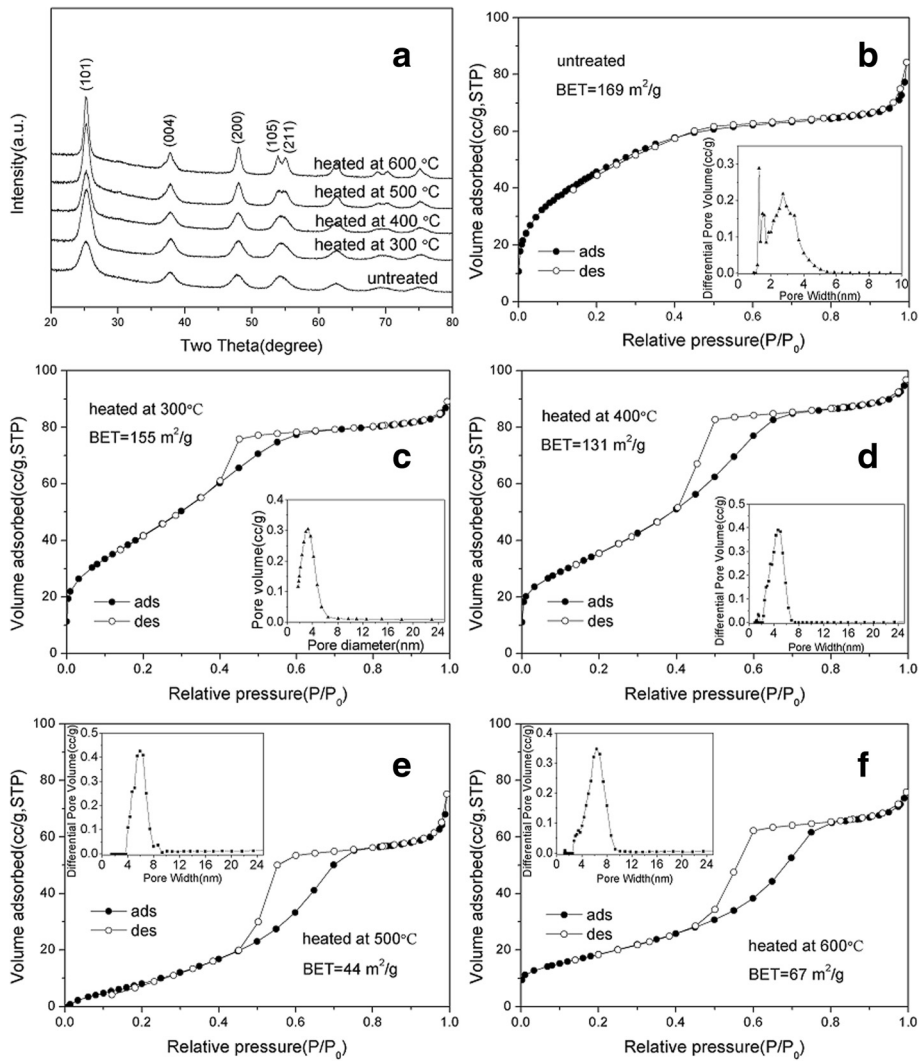

Fig. 5 **a** XRD patterns of TiO_2-NSs. **b**–**f** N_2 adsorption-desorption isotherms and the pore size distribution curves of TiO_2-NSs heated at various temperatures

Moreover, the defect in nano semiconductor photocatalysts plays an important role in photocatalysis [29–31]. The photocatalytic enhancement upon the calcination is attributed to the fact that increasing calcination temperature leads to a decrease in the concentration of bulk defects in TiO_2 due to the increased crystallinity evidenced by XRD (Fig. 5a), thus reducing the recombination of photogenerated electrons and holes. As can be seen from Fig. 6 and Table 2, the specific surface area of the TiO_2-NSs samples decreases with increasing calcination temperature, but actually it should be understood as the increase of the specific photocatalytic activity (per unit surface area), that leads the photocatalytic activity of TiO_2-NSs heated at 400 °C higher than that of uncalcined TiO_2-NSs and other calcinated TiO_2-NSs.

Table 2 Specific surface area, pore size and crystallite size of TiO_2-NSs heated at various temperatures

Sample	Specific surface area (m^2/g)	Average pore size (nm)	Crystallite size (d_{XRD}) (nm)
Untreated	169	1.9	4.6
Heated at 300 °C	155	3.4	5.1
Heated at 400 °C	131	4.7	5.8
Heated at 500 °C	44	5.9	6.9
Heated at 600 °C	67	6.4	9.6

Conclusions

Porous transparent bulk TiO_2 was formed upon slow evaporation of TiO_2-C_2H_5OH colloid. The crystalline building blocks are clearly distinguishable in the free-standing macroscopic bodies. Porous TiO_2-NSs were assembled by refluxing the TiO_2-H_2O colloid and

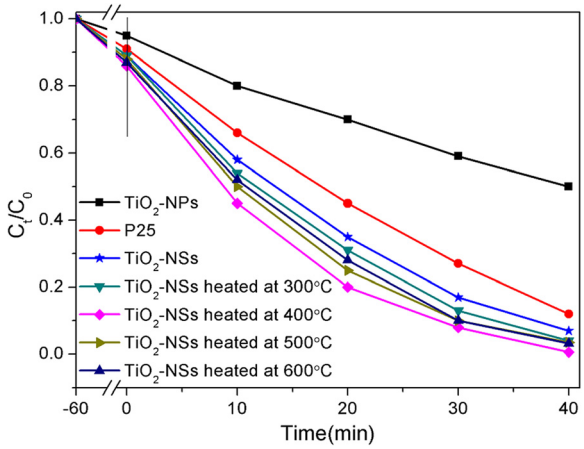

Fig. 6 Photodegradation curves. Photodegradation of MB solutions using TiO_2-NPs (untreated), commercial P25 and TiO_2-NSs heated at various temperatures as photocatalysts under UV irradiation

exhibited enhanced photocatalysis activity compared to the nanoparticles. Both of the porous TiO_2 architectures were pore-size-adjustable depending on the further treating temperature. The current strategy and resulting materials have potentials of designing a variety of bulk objects. The controlled assembly of nanoparticles might open up the pathway to a variety of macroscopic materials with hierarchical architectures and complex morphologies.

Additional File

Additional file 1: Supporting information. **Figure S1.** XRD patterns of TiO_2-NPs. **Figure S2.** TEM image of TiO_2-NPs. **Figure S3.** Size distribution histogram of TiO_2-NPs. **Figure S4.** IR spectrum of the porous transparent bulk TiO_2. **Figure S5.** TG analysis of the porous transparent bulk TiO_2.

Competing Interests
The authors declare that they have no competing interests.

Authors' Contributions
XL undertook the whole research work and prepared the manuscript. WD was involved in the XRD and TEM characterization and analysis of TiO_2 nanoparticles. YC presented the opinion of the thermal stability of porous transparent bulk TiO_2 and was involved in the analysis and measurement of photocatalytic activity. SJ and WX were involved in the analysis and measurement of N_2 adsorption-desorption isotherms. YZ and YK were involved in characterization and preparation of porous transparent bulk TiO_2 and TiO_2-NSs. LL and ZF involved in the SEM and TEM characterization and analysis of the samples. GP designed the experiments and is responsible for the manuscript. All authors read and approved the final manuscript.

Acknowledgements
This work is supported by the National Natural Science Foundation of China (No. 21071058, 21371066, 21301067).

Received: 5 November 2015 Accepted: 14 March 2016
Published online: 22 March 2016

References
1. Dorota K, Alessandro L, Markus N (2014) Metal oxide particles in materials science: addressing all length scales. Adv Mater 26:235–56
2. Pacholski C, Kornowski A, Weller H (2002) Self-assembly of ZnO: from nanodots, to nanorods. Angew Chem Int Ed 41:1188–91
3. Yang J, Peng JJ, Zhang QB, Peng F, Wang HJ, Yu H (2009) One-step synthesis and characterization of gold-hollow PbSx hybrid nanoparticles. Angew Chem Int Ed 48:3991–5
4. Wang X, Fu HB, Peng AD, Zhai TY, Ma Y, Yuan FL, Yao JN (2009) One-pot solution synthesis of cubic cobalt nanoskeletons. Adv Mater 21:1636–40
5. Khalavka Y, Sonnichsen C (2008) Growth of gold tips onto hyperbranched CdTe nanostructures. Adv Mater 20:588–91
6. Sun W, Chen M, Zhou SX, Wu LM (2014) Synthesis of hierarchically nanostructured TiO_2 spheres with tunable morphologies based on a novel amphiphilic polymer precursor and their use for heavy metal ion sequestration. J Mater Chem A 2:14004–13
7. Feng JW, Hong Y, Zhang J, Wang PQ, Hu ZY, Wang Q, Han LY, Zhu YJ (2014) Novel core-shell TiO_2 microsphere scattering layer for dye-sensitized solar cells. J Mater Chem A 2:1502–8
8. Pan JH, Cai ZY, Yu Y, Zhao XS (2011) Controllable synthesis of mesoporous F-TiO_2 spheres for effective photocatalysis. J Mater Chem 21:11430–8
9. Yeom J, Yeom B, Chan H, Smith KW, Dominguez-Medina S, Bahng JH, Zhao GP, Chang WS, Chang SJ, Chuvilin A, Melnikau D, Rogach AL, Zhang PJ, Link S, Kral P, Kotov NA (2015) Chiral templating of self-assembling nanostructures by circularly polarized light. Nat Mater 14:66–72
10. Zhong YR, Yang M, Zhou XL, Luo YT, Wei JP, Zhou Z (2015) Orderly packed anodes for high-power lithium-ion batteries with super-long cycle life: rational design of $MnCO_3$/large-area graphene composites. Adv Mater 27:806–12
11. King NP, Bale JB, Sheffler W, McNamara DE, Gonen S, Gonen T, Yeates TO, Baker D (2014) Accurate design of co-assembling multi-component protein nanomaterials. Nature 510:103–8
12. Oaki Y, Anzai T, Imai H (2010) Homogeneous and disordered assembly of densely packed nanocrystals. Adv Funct Mater 20:4127–32
13. Oaki Y, Nakamura K, Imai H (2012) Homogeneous and disordered assembly of densely packed titanium oxide nanocrystals: an approach to coupled synthesis and assembly in aqueous solution. Chem-Eur J 18:2825–31
14. Shopsowitz KE, Qi H, Hamad WY, MacLachlan MJ (2010) Free-standing mesoporous silica films with tunable chiral nematic structures. Nature 468: 422–U246
15. Ostomel TA, Stucky GD (2004) Free-standing mesoporous titania films with anatase nanocrystallites synthesized at 80 degrees C. Chem Commun 8:1016–7
16. Lou XW, Archer LA (2008) A general route to nonspherical anatase TiO_2 hollow colloids and magnetic multifunctional particles. Adv Mater 20:1853–8
17. Eiden-Assmann S, Widoniak J, Maret G (2004) Synthesis and characterization of porous and nonporous monodisperse colloidal TiO_2 particles. Chem Mater 16:6–11
18. Lv KL, Yu JG, Fan JJ, Jaroniec M (2011) Rugby-like anatase titania hollow nanoparticles with enhanced photocatalytic activity. Cryst Eng Comm 13:7044–8
19. Li HX, Bian ZF, Zhu J, Zhang DQ, Li GS, Huo YN, Li H, Lu YF (2007) Mesoporous titania spheres with tunable chamber structure and enhanced photocatalytic activity. J Am Chem Soc 129:8406–7
20. Li XF, Lv KL, Deng KJ, Tang JF, Su R, Sun J, Chen LQ (2009) Synthesis and characterization of ZnO and TiO_2 hollow spheres with enhanced photoreactivity. Mater Sci Eng B-Adv 158:40–7
21. Liu SW, Yu JG, Mann S (2009) Spontaneous construction of photoactive hollow TiO_2 microspheres and chains. Nanotechnology 20:325606
22. Huang ZA, Wang ZY, Lv KL, Zheng Y, Deng KJ (2013) Transformation of $TiOF_2$ cube to a hollow nanobox assembly from anatase TiO_2 nanosheets with exposed {001} facets via solvothermal strategy. ACS Appl Mater Interface 5:8663–9
23. Innocenzi P, Malfatti L, Kldchob T, Falcaro P (2009) Order-disorder in self-assembled mesostructured silica films: a concepts review. Chem Mater 21:2555–64
24. Wang DP, Zeng HC (2009) Multifunctional roles of TiO_2 nanoparticles for architecture of complex core-shells and hollow spheres of SiO_2-TiO_2-polyaniline system. Chem Mater 21:4811–23
25. Chen DH, Cao L, Huang FZ, Imperia P, Cheng YB, Caruso RA (2010) Synthesis of monodisperse mesoporous titania beads with controllable diameter, high surface areas, and variable pore diameters (14-23 nm). J Am Chem Soc 132: 4438–44

26. Zhang Z, Wang CC, Zakaria R, Ying JY (1998) Role of particle size in nanocrystalline TiO_2-based photocatalysts. J Phy Chem B 102:10871–8
27. Wang CC, Zhang Z, Ying JY (1997) Photocatalytic decomposition of halogenated organics over nanocrystalline titania. Nanostruct Mater 9: 583–6
28. Bisquert J, Zaban A, Salvador P (2002) Analysis of the mechanisms of electron recombination in nanoporous TiO_2 dye-sensitized solar cells. Nonequilibrium steady-state statistics and interfacial electron transfer via surface states. J Phy Chem B 106:8774–82
29. Kong M, Li YZ, Chen X, Tian TT, Fang PF, Zheng F, Zhao XJ (2011) Tuning the relative concentration ratio of bulk defects to surface defects in TiO_2 nanocrystals leads to high photocatalytic efficiency. J Am Chem Soc 133:16414–7
30. Li YZ, Xie W, Hu XL, Shen GF, Zhou X, Xiang Y, Zhao XJ, Fang PF (2010) Comparison of dye photodegradation and its coupling with light-to-electricity conversion over TiO_2 and ZnO. Langmuir 26:591–7
31. Xie W, Li YZ, Sun W, Huang JC, Xie H, Zhao XJ (2010) Surface modification of ZnO with Ag improves its photocatalytic efficiency and photostability. J Photoch Photobio A 216:149–55